Environmental Science
Processes & Impacts

Accepted Manuscript

ROYAL SOCIETY OF CHEMISTRY

rsc.li/process-impacts

Redox Activity and Chemical Interaction of Metal Oxide Nano- and Micro- Particles with Dithiothreitol (DTT)

Johny Nicolas,[1] Malek Jaafar,[1] Elizabeth Sepetdjian,[1] Walid Saad,[2] Constantinos Sioutas,[3] Alan Shihadeh,[4] and Najat A. Saliba.[1]*

[1] American University of Beirut, Lebanon, Chemistry Department, Faculty of Arts and Sciences

[2] American University of Beirut, Lebanon, Department of Chemical and Petroleum Engineering, Faculty of Engineering and Architecture

[3]University of Southern California, Department of Civil and Environmental Engineering, Los Angeles, USA

[4]American University of Beirut, Lebanon, Mechanical Engineering Department, Faculty of Engineering and Architecture

*Corresponding Author: Najat Saliba, Ph.D., American University of Beirut, Beirut, Lebanon. E-mail: ns30@aub.edu.lb

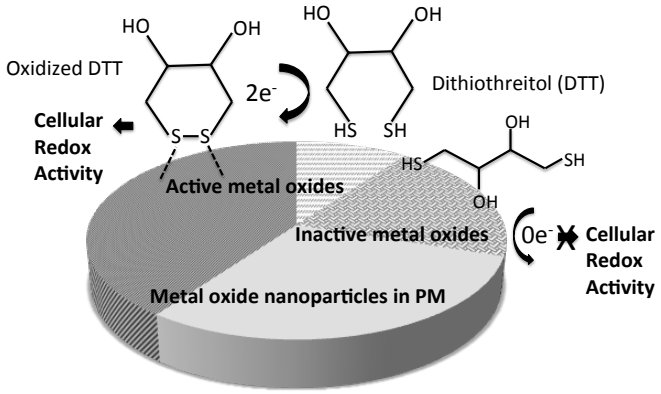

Redox Activity and Chemical Interaction of Metal Oxide Nano- and Micro- Particles with Dithiothreitol (DTT)

Johny Nicolas,[1] Malek Jaafar,[1] Elizabeth Sepetdjian,[1] Walid Saad,[2] Constantinos Sioutas,[3] Alan Shihadeh,[4] and Najat A. Saliba.[1]*
[1] American University of Beirut, Lebanon, Chemistry Department, Faculty of Arts and Sciences
[2] American University of Beirut, Lebanon, Department of Chemical and Petroleum Engineering, Faculty of Engineering and Architecture
[3]University of Southern California, Department of Civil and Environmental Engineering, Los Angeles, USA
[4]American University of Beirut, Lebanon, Mechanical Engineering Department, Faculty of Engineering and Architecture

*Corresponding Author: Najat Saliba, Ph.D., American University of Beirut, Beirut, Lebanon. E-mail: ns30@aub.edu.lb

Abstract

The wide application and production of nanotechnology has increased the interest in studying the toxicity of nano- and micro-sized particles escaping into the air from various aspects of the production process. Metal oxides (MO) are one particular class of particles that exist abundantly in ambient PM. Studies show emphasis on biological mechanisms by which inhalation exposure to MO lead to disease. However, different biological assays provide different redox activity rankings making it difficult to assess the contributions of various MO to measures of aggregate toxicity in multi-pollutant systems such as ambient PM. Therefore, research to evaluate the chemical interaction between these particles and molecules that are relevant to cellular redox activity can help in establishing indicators of reactivity. In particular, this study assesses the redox activity of six MO mainly emitted from anthropogenic industrial activities using the dithiothreitol (DTT) assay. DTT is commonly used in acellular assays due to its analogous structure to cellular glutathione. The structural and chemical behaviors between active MOs and DTT were elucidated using FTIR, NMR, and BET methods. Results indicate that the health risk (redox activity) associated with MO is mainly a function of its surface reactivity demonstrated by the ability of oxidized (S-H) bond in DTT to form a stable bond with the MO surface.

Introduction

The wide application and full-scale production of nanotechnology has increased the interest in studying the toxicity of nano- and micro-sized particles escaping into the air from various aspects of the production process. Metal oxides (MO) are one particular class of ~~nano~~particles that exist abundantly in ambient PM. Several studies have predicted the toxicity of these particles using cellular and acellular assays.[1-5] Various deleterious health outcomes, including inflammation and cancer, have been associated with inhalation exposure to MO because of their ability to induce oxidative stress in cells.[6-8] However, different assays provide different redox activity rankings,[9, 10] making it difficult to assess the contributions of various MO to measures of aggregate toxicity in multi-pollutant systems such as ambient PM. More work on the chemical and biological mechanisms involved in MO redox is needed to resolve the apparent contradictions across assays.

Biological mechanisms of MO particles have been investigated in several studies. Most of these studies address the changes in cell-to-cell signaling as well as in the expression of transcription factors in presence of MO; others investigate alterations in mitochondria function in cells [11-17] Comparatively, few studies have addressed the chemical interactions and the structural changes in biological molecules that occur upon interaction with MO. As an example of a chemical explanation for the toxicity of MO, Burello and Worth [17-19] showed that if the band gap of the MO overlaps with the band gap of the redox potentials of biological reactions occurring inside cells, then the MO is capable of unbalancing the cellular redox state and ultimately induce oxidative stress in the cells. Applying this theory to the growth inhibitory effects of 24 MO nanoparticles in mammalian cells and the bacterium Escherichia coli, it was found that ZnO, CuO, CoO, Mn_2O_3, Co_3O_4, Ni_2O_3, and Cr_2O_3, induce oxidative stress to the system in question. Other physicochemical parameters such as the hydration enthalpy becoming less negative [20] and the solubility of MO [21-23] were correlated

to the toxicological data with MO.

In this study, the dithiothreitol (DTT) assay is used. This assay relies on the transformation of DTT to its oxidized form by redox-active MO. There are two main reasons that make this assay relevant for chemical biology studies. First, the DTT reaction in vitro resembles the Nicotinamide Adenine Dinucleotide (NADH) oxidation reaction in vivo in which NADH is also transformed to its oxidized form NAD^+ (Figure 1): the capacity of metal oxide to induce the transfer of electron from DTT (or NADH) to O_2 is tested.[24] Second, the dithiothreitol resembles glutathione, an important antioxidant involved in scavenging reactive oxygen species and in preventing inflammatory reactions in cells.

The DTT assay was used to determine the oxidative potential of six MO (CuO, MnO_2, ZnO, PbO, Pb_3O_4 and Cr_2O_3) commonly found in ambient PM. To the authors' knowledge, apart from lead oxide,[25] there are no literature values reported for the reactivity of DTT and the selected MO. It was hypothesized that the solubility, the overlap between the band gap of MO and the one of the redox potential of biological molecules, and the enthalpy of hydration of MO play a major factor in increasing the toxicity of these particles in cells. To test the contribution of other factors like MO active surface area, several spectroscopic techniques including Fourier Transform Infra Red (FTIR), Hydrogen Nuclear Magnetic Resonance (1H-NMR), Brunauer–Emmett–Teller (BET), Scanning Electron Microscopy (SEM) and Dynamic Light Scattering (DLS) were used to probe the mechanism of interaction between non-soluble MO suspended in methanol and DTT.

Experimental

MO were purchased from analytical grade manufacturers (lead oxides were purchased from Mallinckrodt Chemical Inc., chromium oxide from JT-Baker, zinc oxide from Analar

analytical reagents, manganese oxides from Merck and copper oxide from Reidel-de-Haen chemical company). The physical characteristics of the MO powder were characterized using several analytical techniques, including DLS, SEM coupled with Energy Dispersive X-ray system (EDX), and BET as detailed below.

Solution Preparation and Analytical Measurements

MO solutions for the above mentioned species were prepared by suspending the required mass for 1 mM in 20 mL methanol. In addition a 25 μM Copper II Chloride ($CuCl_2$) methanolic solution was prepared as a positive control for the DTT assay, as mentioned later.

Dynamic Light Scattering (DLS): In order to characterize particle size distributions of the MO, solutions were prepared by weighing 1 mg of each MO in 25 mL methanol followed by up to 100 times dilution depending on the response of DLS instrument (90Plus, Brookhaven Instruments Corporation). Lead oxides were not analyzed due to rapid settling of the samples. MO suspensions were analyzed at 90° scattering and 25°C with each run was repeated in triplicate. The primary result provided by the instrument is the autocorrelation function, which was converted to intensity-weighted differential size distribution using the Non-Negatively constrained Least Squares (NNLS) algorithm.

Scanning Electron Microscopy (SEM): MO particles suspended in methanol and MO mixed with DTT were examined using SEM (Tescan Model 51-XMX0010) equipped with an EDX system for elemental identification. SEM operated at 20-30 KeV and 60 μA beam current, with spectral acquisition time of 60 sec. A mass of approximately 1.0 g of each MO was used in this analysis; mineral oxides particles were taken directly from manufacturer containers without being suspended in methanol.

The dithiothreitol (DTT) Assay: An optimized DTT assay reported by Li et al. (2009)[26] was adapted for this study. Methanol was the solvent of choice because it is commonly used in PM-DTT studies.[27, 28] However, because MO are insoluble in methanol, the experiments were conducted in-situ in order to avoid the need to withdraw aliquots from the solution. As such, the volumes and concentrations of the DTT, 5,5'-dithiobis-(2-nitrobenzoic acid) (DTNB) and phosphate buffer had to be increased to account for the large volume of the samples.

The modified method consists of sonicating for 30 minutes suspended MO solutions, prior to the experiment. The solution was then mixed with 100 ml of 0.1 M phosphate buffer, followed by the addition of 5 mL of 1 mM DTT. The mixture was placed in a water bath incubator/shaker (37°C, 180 rpm) throughout the experiment to ensure homogeneity. At the optimized 8, 12 and 16 sec, 1 mL of the mixture was taken out and added to 1 ml of 1.5 mM DTNB. The yellow 2-nitro-5-thiobenzoate (TNB) solution was measured within 1 hour of the experiment's completion using a UV/Vis spectrophotometer (JASCO V-570 UV/VIS/NIR Spectrophotometer). The rate loss was calculated by plotting the absorbance of the DTNB at 412 nm versus the optimized time of the experiment mentioned above. The slope of the straight line represented the DTT rate loss (nmole/min) of the MO in question. In order to normalize between the different masses of the MO, rate losses were divided by the weighed mass (nmole/min μg). The MO reactivity towards DTT assay was assessed three times and for each experiment the MO-DTT reaction was run in triplicates.

Fourier Transform Infra Red (FTIR) and Nuclear Magnetic Resonance (NMR) spectroscopy: For FTIR and NMR spectroscopy, the solutions were sonicated for 30 minutes before the addition of DTT and incubated after adding DTT for 30 minutes at a temperature of 37°C.

Then, solvents were evaporated using a vacuum rotary evaporator and residues were either mixed with KBr and pressed into a transparent pellet for FTIR or resuspended in d-methanol for NMR analyses. For FTIR, a Nicolet AVATAR 360 FTIR spectrometer equipped with a KBr pellet cell holder was used to collect FTIR spectra by averaging 254 scans at wavenumbers ranging from 600 to 4000 cm^{-1} at a resolution of 1 cm^{-1} and for NMR, a Bruker 400 MHz spectrometer was used to record one-dimensional 1H. The chemical shifts are reported in ppm values relative to the internal standard tetramethylsilane (TMS).

Brunauer–Emmett–Teller (*BET):* The surface area of all MO was measured using the BET isotherm. Prior to analysis, MO samples were degased for 4 hours at a temperature of 300°C. A mass of approximately 1.0 g of each MO was used in this analysis; MO particles were taken directly from manufacturer containers without being suspended in methanol. A Surface Area Analyzer (Quantachrome NOVA 2200e Surface Area & Pore Size Analyzer) was used to collect the BET isotherm.

Results and Discussion

The physical and chemical variations of MO nano- and micro-sized particles in solution and reaction media are studied using several spectroscopic techniques. Results are summarized in Table 1. The analysis of the presented data led to proposing a reaction mechanism and associated structure modifications.

Particle size distribution and surface area

Particle diameters of the tested commercial MOs (CuO, MnO_2, ZnO, PbO, Pb_3O_4 and Cr_2O_3) were measured using SEM (Figure S1 and Table S1) and DLS. SEM is useful in giving single particle size while DLS measures the size of an agglomeration of particles in solution;

hence the discrepancy in results between the two techniques. In solution, the deviation from the nanoparticle sizes during DLS measurements is evident as commercial MOs do not necessarily recover their primary particle size upon solvent dispersion due to solvation, aggregation and other instabilities[29] Diameters of 100 mineral oxide particles (100 for each of the 6 different metal oxides) calculated based on SEM images ranged between 0.060 and 0.110 μm, with an average of 0.0792 ± 0.0068 μm. Solvated particle diameters in methanol, which were measured using DLS, varied between 0.200 and 0.400 μm for Cr_2O_3, MnO_2 and CuO. Particle diameters of ZnO in solution showed a wider particle diameter of 1.64 ± 0.87 μm and lead oxides particles could not be measured using DLS due to rapid settling. A summary of the results is shown in Table 1.

DTT redox activity

As shown in Figure 2, the MO redox activities (per mass) in decreasing order are: CuO> MnO_2 ~ ZnO>PbO>Pb_3O_4>Cr_2O_3. The activity of CuO is similar to the positive control (Cu^{2+}), Pb_3O_4 is 88.3% lower than CuO, and Cr_2O_3 exhibits no reactivity towards DTT. When normalized to the MO surface area, the order of redox activity becomes MnO_2>PbO>CuO>Pb_3O_4>ZnO>Cr_2O_3 with the activity of MnO_2, CuO, and PbO being one order of magnitude higher than the activity per surface area of Pb_3O_4 and ZnO (shown in the insert of Figure 2). Active surfaces seem to provide binding sites able to oxidize DTT (Figure S2). These results are in line with the proposed mechanism of interaction based on the FTIR and NMR data shown below.

IR and NMR Spectra

Infrared assigned peaks of oxidized DTT are shown in Figures 3 and 4 and summarized in Table S3. NMR spectra are displayed in Figure 5.

DTT

The IR spectrum of the DTT solution (Figures 3 and 4) shows a C-S band at 677 cm^{-1}. The two peaks at 1054 and 1101 cm^{-1} are attributable to vibrational modes of C-O stretch (Figure 3). The peak at 1408 cm^{-1} can be assigned to CH_2 scissoring mode, while weak bands between 1320 and 1230 arise from CH_2 vibrations and weak peaks ranging between 2970 and 2910 cm^{-1} are attributed to C-H stretching bands. The two equal intensity peaks at 2564 and 2547 cm^{-1} are typical of S-H stretch (Figure 4). These peaks may be assigned to DTT hydrogen-bonded dimers and monomers, respectively. Contrary to S-H, OH stretching vibration shows one broad peak at 3360 cm^{-1} attributed to hydrogen bonding with methanol (solvent).[30]

CuO-, MnO_2-, PbO-DTT

Spectra of oxidized DTT by CuO, MnO_2 and PbO show no peaks in the 2540-2570 cm^{-1} region typical of S-H stretch, indicating that oxidation of DTT by these MO occurs with thiol deprotonation. The two C-S peaks at 746 and 756 cm^{-1}depend on the molecular conformations about the C-C bonds adjacent to the C-S bonds and are assigned to the *v*(C-S) stretch of the *Gauch* and *Trans*forms, respectively.[31, 32] The new peak at 791 cm^{-1} is attributed to CH_2 rocking attached to disulfide.[33, 34] The peaks in the 975 - 1040 cm^{-1} region particularly at 994, 1008, and 1036 cm^{-1} are significantly different from those of the solution prior to adding DTT. These bands are assigned to *v*(C-C) vibrations with an enhanced and sharp *Trans v*(C-C) band at 1036 cm^{-1}. The band at 1060 cm^{-1} is attributed to *v*(C-O) vibration. The cyclic disulfide form of DTT is further supported by the presence of twisting-rocking and wagging bands located between 1100 and 1375 cm^{-1} and the appearance of a sharp scissoring band of the methylene groups at 1453 cm^{-1}. The CH_2 scissoring mode at 1453 cm^{-}

[1] is offset in absorbance when compared to the DTT solution. These sharp bands are typical of disulfide DTT adsorbed on metal surfaces.[35, 36] The IR spectrum of oxidized DTT (Figure 4), shows the asymmetric and symmetric stretching bands of CH_2 ($\nu(CH_2)$) sharpen and redshift to 2873, 2909, 2930 and 2956 cm^{-1}. The presence of four bands for $\nu(CH_2)$ corroborates the presence of a *Gauch* and *Trans* conformations.[36] The sharpening of the peaks further indicates the increase in the crystallinity of oxidized DTT on the MO surface. In the O-H region (3330-3500 cm^{-1}), two fairly sharp peaks are observed. The un-bonded OH gives rise to the minor peak at 3430 cm^{-1}, and the major band at 3303 cm^{-1} provides evidence that the intra-molecularly bonded species must also be present.[37, 38]

The 1H-NMR data with broad CH_2 and CH peaks in the regions of 2.80-2.95 and 2.96-3.10 ppm (insert of Figure 5) also confirms that two conformers of oxidized DTT are formed at the surface (Figure 5).

Pb_3O_4- and ZnO-DTT

The IR spectra of Pb_3O_4- and ZnO-DTT show only one thiol ν(S-H) at 2564 cm^{-1} and one broad ν(C-S) peak at 738 cm^{-1} (Figures 3 & 4). This indicates either the co-presence of DTT and oxidized DTT (S-S bond formation) in solution or the presence of the partially oxidized DTT with one S-H and one MO-S bond. The peaks in the 975 - 1500 cm^{-1} and 2800 - 3000 cm^{-1} regions show a combination of DTT and oxidized DTT peaks. The O-H single peak at 3390 cm^{-1} is broader than the OH peak of DTT in solution suggesting again the occurrence of the thiol (S-H) and oxidized form of DTT (MO-S). The fact that the peak is downshifted by 30 cm^{-1} even for unreacted Cr_2O_3 indicates the enhancement of hydrogen bonding upon adsorption. 1H-NMR spectra of Pb_3O_4 and CuO as shown in Figure 5 confirms the suggested co-presence of thiol (S-H) and oxidized DTT (MO-S) in solution. Results infer the limited

reactivity of these MO towards DTT due to the limited or partial oxidation of DTT. All analytical measurements also support the conclusion of DTT not reacting with Cr_2O_3.

Two main reactivity patterns have been observed between the six MOs that were studied and DTT. The higher activity of CuO, MnO_2 and PbO was correlated with a chemisorbed disulfide ordered structure on the MO surfaces as confirmed by IR and 1H-NMR data. Pb_3O_4 and ZnO, showed lower reactivity towards DTT with the IR and 1H-NMR spectra revealing the co-presence of the thiol (S-H) and oxidized DTT (MO-S) bonds. It has been reported that the modes of interaction between MO and DTT can proceed via a surface catalytic pathway, reduction of the dissolved metal ion and the oxidation of the thiol (HSR) group to the corresponding disulfide (RS-SR), or electron transfer leading to the formation of a stable ligand between the metal ion and oxidized DTT.[31, 32, 39-43] In this study, it is suggested that the two reactivity patterns follow a surface catalytic Fenton-like pathway with higher activity MO surfaces forming ordered chemisorbed layers of fully oxidized DTT (RS-SR) while the ones with lower reactivity leading to the partially oxidized form (RS-SH) of DTT.

The increase in anthropogenic emissions of MO ~~nano~~particles into the atmosphere calls for the understanding of their oxidative effects on human cells. In this study, an a-cellular assay of DTT reaction with some abundant MO like CuO, MnO_2, ZnO, PbO, Pb_3O_4 and Cr_2O_3 has been used to model their effects on sulfur-containing biological molecules such as glutathione. By understanding the structural changes that occur to DTT, we were able to explain the difference in activities of the various MO. The mass-normalized reactivity of MO toward DTT was assessed and determined to be in the following ranking: $CuO>MnO_2{\sim}ZnO>PbO>Pb_3O_4>Cr_2O_3$. When normalized to the surface area calculated with BET the reactivity order becomes $MnO_2>PbO>CuO>Pb_3O_4>ZnO>Cr_2O_3$ with MnO_2, PbO,

and CuO reactivities being one order of magnitude higher than Pb_3O_4 and ZnO. Based on IR and 1H-NMR spectroscopic analysis, it was found that active surface areas of MnO_2, PbO, and CuO lead to a complete catalytic oxidization of DTT and to chemical bond between oxidized DTT and the MO surface via the disulfide bond. Limited reactivity of Pb_3O_4 and ZnO suggests a similar pathway of catalytic Fenton like reaction leading to a single bonded DTT to the surface via the HS-RS-MO bond.

Acknowledgements

This work has been supported by the American University Research Board (URB).

References

1. S. M. Hussain, K. L. Hess, J. M. Gearhart, K. T. Geiss and J. J. Schlager, *Toxicology in Vitro*, 2005, **19**, 975-983.
2. X. Hu, S. Cook, P. Wang and H.-m. Hwang, *Science of The Total Environment*, 2009, **407**, 3070-3072.
3. J. Choi, S. Lee, H. Na, K. An, T. Hyeon and T. Seo, *Bioprocess Biosyst Eng*, 2010, **33**, 21-30.
4. A. L. Holder, R. Goth-Goldstein, D. Lucas and C. P. Koshland, *Chemical Research in Toxicology*, 2012, **25**, 1885-1892.
5. P. Møller, D. M. Jensen, D. V. Christophersen, A. Kermanizadeh, N. R. Jacobsen, J. G. Hemmingsen, P. H. Danielsen, D. G. Karottki, M. Roursgaard, Y. Cao, K. Jantzen, H. Klingberg, L.-G. Hersoug and S. Loft, *Environmental and Molecular Mutagenesis*, 2015, **56**, 97-110.
6. W. Lin, Y.-w. Huang, X.-D. Zhou and Y. Ma, *International Journal of Toxicology*, 2006, **25**, 451-457.
7. A. Gojova, B. Guo, R. S. Kota, J. C. Rutledge, I. M. Kennedy and A. I. Barakat, *Environmental Health Perspectives*, 2007, **115**, 403-409.
8. W. S. Cho, R. Duffin, C. A. Poland, S. E. Howie, W. MacNee, M. Bradley, I. L. Megson and K. Donaldson, *Environ Health Perspect*, 2010, **118**, 1699-1706.
9. V. Aruoja, H.-C. Dubourguier, K. Kasemets and A. Kahru, *Science of The Total Environment*, 2009, **407**, 1461-1468.
10. Y.-W. Baek and Y.-J. An, *Science of The Total Environment*, 2011, **409**, 1603-1608.
11. M. A. A. Schoonen, C. A. Cohn, E. Roemer, R. Laffers, S. R. Simon and T. O'Riordan, *Reviews in Mineralogy and Geochemistry*, 2006, **64**, 179-221.
12. S. V, H. Johnston and M. Clift, *IEEE Transactions on Nanobioscience*, 2007, **6**, 331-340.
13. J. Zhao, L. Bowman, X. Zhang, V. Vallyathan, S. H. Young, V. Castranova and M. Ding, *Journal of toxicology and environmental health. Part A*, 2009, **72**, 1141-1149.
14. H.-J. Eom and J. Choi, *Environmental Science & Technology*, 2010, **44**, 8337-8342.
15. H. J. Johnston, G. Hutchison, F. M. Christensen, S. Peters, S. Hankin and V. Stone, *Critical Reviews in Toxicology*, 2010, **40**, 328-346.
16. M. I. Khan, A. Mohammad, G. Patil, S. A. Naqvi, L. K. Chauhan and I. Ahmad, *Biomaterials*, 2012, **33**, 1477-1488.
17. H. Zhang, Z. Ji, T. Xia, H. Meng, C. Low-Kam, R. Liu, S. Pokhrel, S. Lin, X. Wang, Y.-P. Liao, M. Wang, L. Li, R. Rallo, R. Damoiseaux, D. Telesca, L. Mädler, Y. Cohen, J. I. Zink and A. E. Nel, *ACS Nano*, 2012, **6**, 4349-4368.
18. E. Burello and A. P. Worth, *Nanotoxicology*, 2010, **5**, 228-235.
19. E. Burello and A. P. Worth, *Wiley Interdisciplinary Reviews: Nanomedicine and Nanobiotechnology*, 2011, **3**, 298-306.
20. C. Kaweeteerawat, A. Ivask, R. Liu, H. Zhang, C. H. Chang, C. Low-Kam, H. Fischer, Z. Ji, S. Pokhrel, Y. Cohen, D. Telesca, J. Zink, L. Mädler, P. A. Holden, A. Nel and H. Godwin, *Environmental Science & Technology*, 2015, **49**, 1105-1112.
21. T. J. Brunner, P. Wick, P. Manser, P. Spohn, R. N. Grass, L. K. Limbach, A. Bruinink and W. J. Stark, *Environmental Science & Technology*, 2006, **40**, 4374-4381.

22. T. Xia, M. Kovochich, M. Liong, L. Mädler, B. Gilbert, H. Shi, J. I. Yeh, J. I. Zink and A. E. Nel, *ACS Nano*, 2008, **2**, 2121-2134.
23. M. Pandurangan and D. Kim, *J Nanopart Res*, 2015, **17**, 1-8.
24. V. Verma, Doctor of Philosophy University of Southern California 2011.
25. G. Uzu, J.-J. Sauvain, A. Baeza-Squiban, M. Riediker, M. Sánchez Sandoval Hohl, S. Val, K. Tack, S. Denys, P. Pradère and C. Dumat, *Environmental Science & Technology*, 2011, **45**, 7888-7895.
26. N. Li, M. Wang, L. A. Bramble, D. A. Schmitz, J. J. Schauer, C. Sioutas, J. R. Harkema and A. E. Nel, *Environmental Health Perspectives*, 2009, **117**, 1116-1123.
27. W. Rattanavaraha, E. Rosen, H. Zhang, Q. Li, K. Pantong and R. M. Kamens, *Atmospheric Environment*, 2011, **45**, 3848-3855.
28. V. Verma, R. Rico-Martinez, N. Kotra, L. King, J. Liu, T. W. Snell and R. J. Weber, *Environmental Science & Technology*, 2012, **46**, 11384-11392.
29. Y. Zhang, Y. Chen, P. Westerhoff, K. Hristovski and J. C. Crittenden, *Water research*, 2008, **42**, 2204-2212.
30. J. G. David and H. E. Hallam, *Spectrochimica Acta*, 1965, **21**, 841-850.
31. H. Sugeta, A. Go and T. Miyazawa, *Chemistry Letters*, 1972, **1**, 83-86.
32. Y.-S. Li, Y. Wang, J. S. Church, F. Garzena, Z. Zhang and D. An, *Spectrochimica Acta Part A: Molecular and Biomolecular Spectroscopy*, 2003, **59**, 1791-1798.
33. T. Hayashi, C. Kodama and H. Nozoye, *Applied Surface Science*, 2001, **169–170**, 100-103.
34. O. Furlong, B. Miller, Z. Li and W. T. Tysoe, *Surface Science*, 2011, **605**, 606-611.
35. L. A. Porter, D. Ji, S. L. Westcott, M. Graupe, R. S. Czernuszewicz, N. J. Halas and T. R. Lee, *Langmuir*, 1998, **14**, 7378-7386.
36. B. S. Zelakiewicz, G. C. Lica, M. L. Deacon and Tong, *Journal of the American Chemical Society*, 2004, **126**, 10053-10058.
37. A. W. Baker and A. T. Shulgin, *Journal of the American Chemical Society*, 1958, **80**, 5358-5363.
38. R. J. Abraham and M. Mobli, *Magnetic Resonance in Chemistry*, 2007, **45**, 865-877.
39. H. Keller, P. Simak, W. Schrepp and J. Dembowski, *Thin Solid Films*, 1994, **244**, 799-805.
40. P. J. Unwin, M. E. Rusnacik, S. M. Kresta and A. E. Nelson, *Colloids and Surfaces A: Physicochemical and Engineering Aspects*, 2008, **325**, 72-80.
41. A. G. Young, D. P. Green and A. J. McQuillan, *Langmuir*, 2007, **23**, 12923-12931.
42. A. Ulman, S. D. Evans, Y. Shnidman, R. Sharma, J. E. Eilers and J. C. Chang, *Journal of the American Chemical Society*, 1991, **113**, 1499-1506.
43. K. L. Prime and G. M. Whitesides, *Science*, 1991, **252**, 1164-1167.

Table 1. Physical characteristics (surface area and particle diameter) of metal oxide particles and their reactivity towards DTT

Metal Oxide	**DTT rate loss (nmol/min µg)**	**Surface Area (m^2)**	**DTT rate loss/Surface Area ((nmol/min µg m^2)**	**Particle Diameter (µm)**
$CuCl_2$	0.86	NA* due to ionic character	NA due to ionic character	NA due to ionic character
CuO	0.80	30.7	0.0262	0.219 ± 0.116
MnO_2	0.30	7.5	0.0406	0.370 ± 0.066
ZnO	0.25	137	0.0018	1.64 ± 0.87
PbO	0.14	3.7	0.0392	NA due to rapid settling
Pb_3O_4	0.01	3.9	0.0036	NA due to rapid settling
Cr_2O_3	-0.02	6.5	-0.0031	0.377 ± 0.061

NA stands for not available

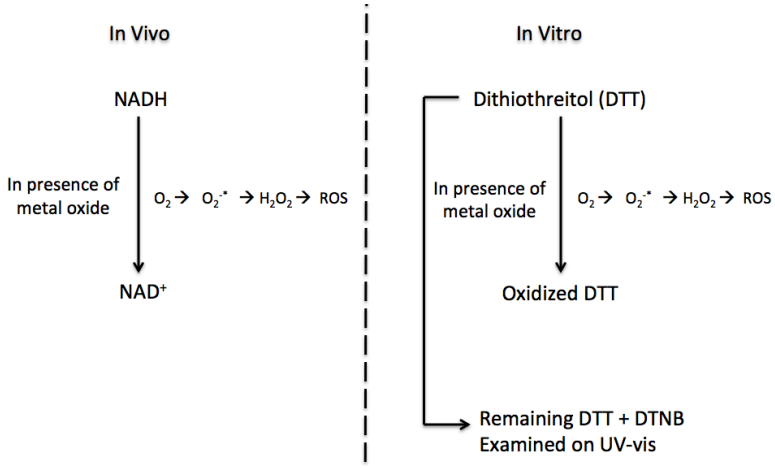

Figure 1. DTT reaction mechanism and its resemblance to the NADH transformation in cells to generate ROS

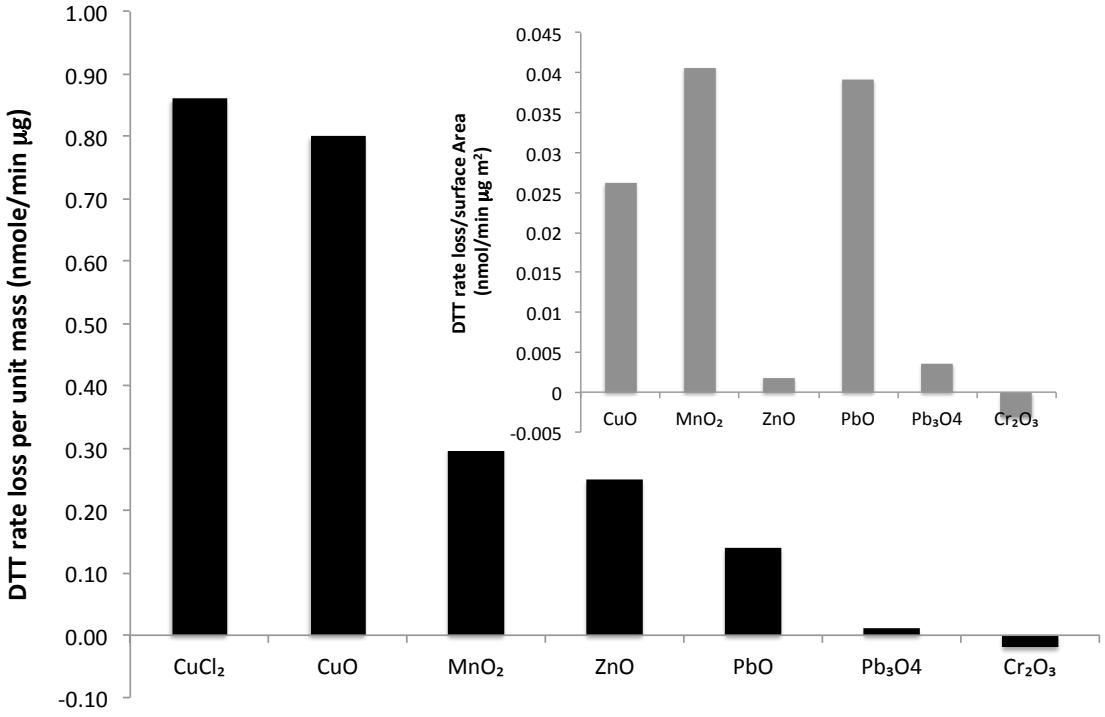

Figure 2. DTT rate loss (nmole/min μg) for MO particles normalized to mass of MO. The insert shows DTT rate loss (nmole/min μg m^2) for MO particles normalized to the particle surface area and the mass of MO

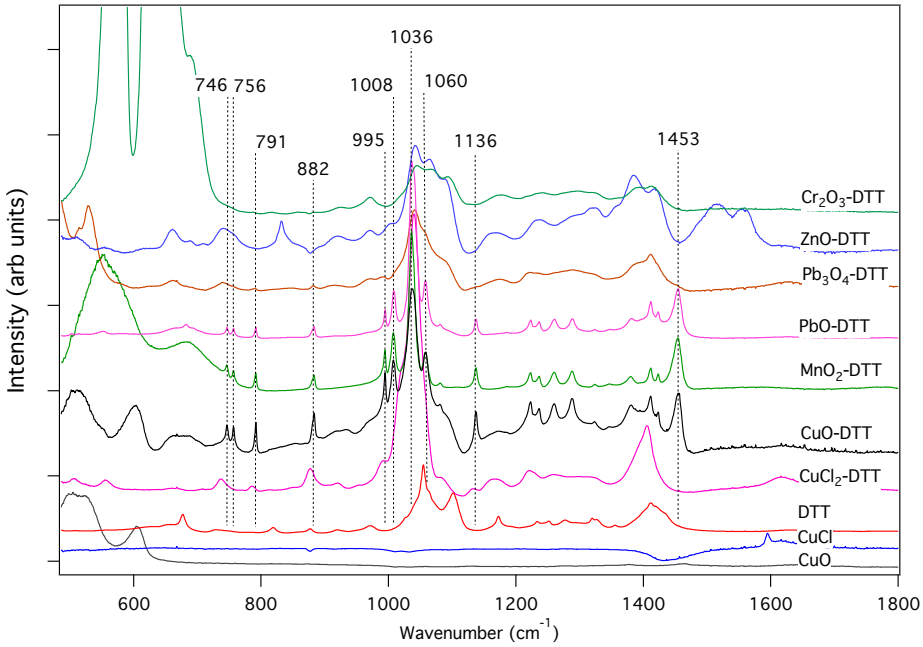

Figure 3. Infrared spectra in the 500-1800 cm^{-1} range of CuO, $CuCl_2$, dithiothreitol (DTT), oxidized DTT by $CuCl_2$ ($CuCl_2$-DTT), and products of DTT-metal oxides (CuO, MnO_2, PbO, Pb_3O4, ZnO, and Cr_2O_3) reactions

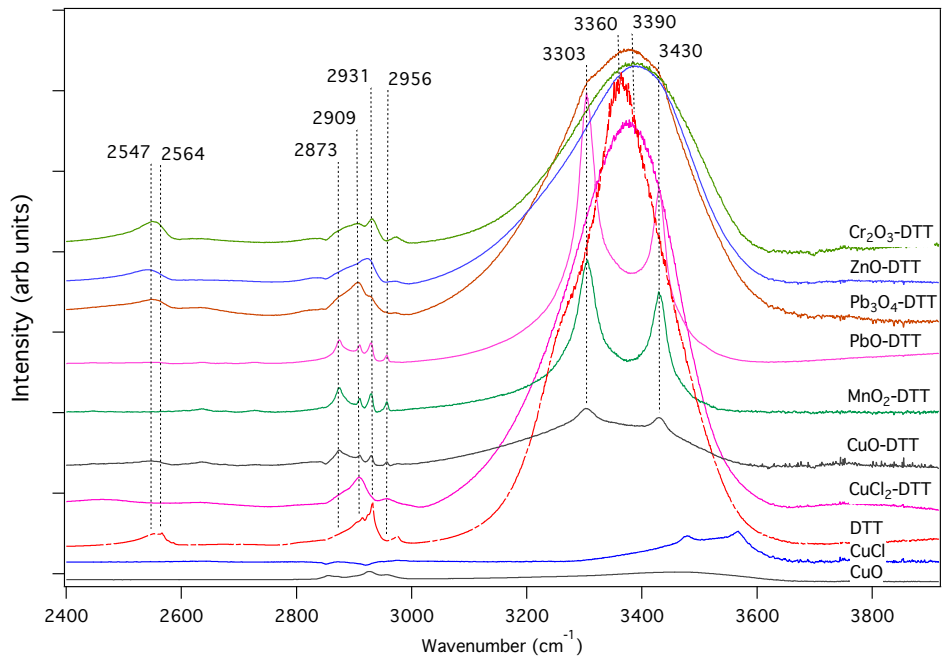

Figure 4. Infrared spectra in the 2400-3900 cm^{-1} range of CuO, $CuCl_2$, dithiothreitol (DTT), oxidized DTT by $CuCl_2$ ($CuCl_2$-DTT), and products of DTT-metal oxides (CuO, MnO_2, PbO, Pb_3O4, ZnO, and Cr_2O_3) reactions

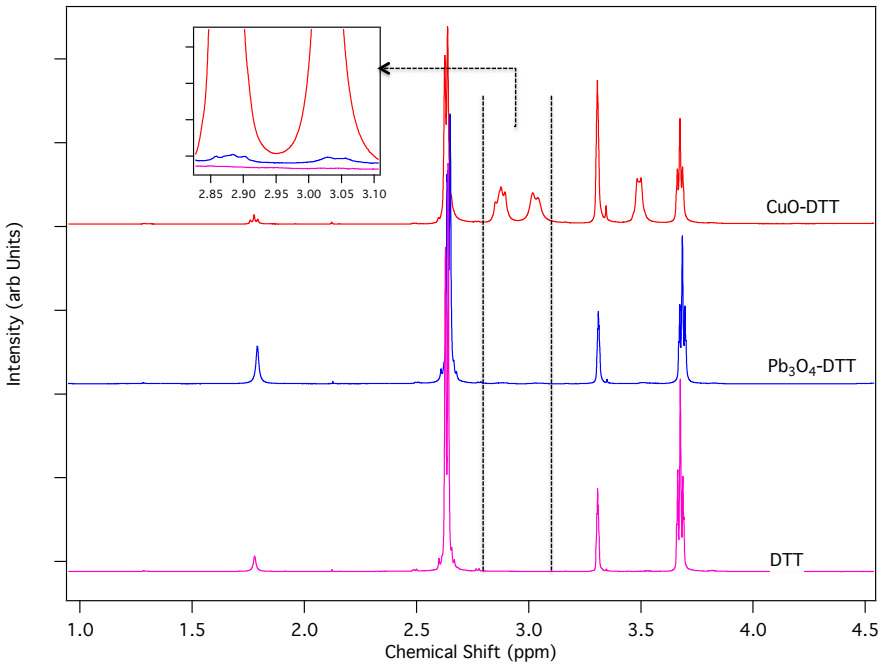

Figure 5. Hydrogen Nuclear Magnetic Resonance (1H-NMR) spectra of dithiothreitol (DTT), Pb_3O_4-DTT, and CuO-DTT reactive mixtures